IEEE Access
Multidisciplinary | Rapid Review | Open Access Journal

Received April 23, 2018, accepted June 25, 2018, date of publication June 29, 2018, date of current version July 30, 2018.

Digital Object Identifier 10.1109/ACCESS.2018.2851591

Improved Energy Efficiency of Massive MIMO-OFDM in Battery-Limited IoT Networks

BYUNG MOO LEE, (Member, IEEE)
School of Intelligent Mechatronics Engineering, Sejong University, Seoul 05006, South Korea
e-mail: blee@sejong.ac.kr

This work was supported by the Basic Science Research Program through the National Research Foundation of Korea funded by the Ministry of Education under Grant NRF-2017R1D1A1B03028350.

ABSTRACT We investigate the feasibility of improving the energy efficiency (EE) of massive multiple-input multiple-output (MIMO) orthogonal frequency division multiplexing (OFDM) systems applied to a battery-limited Internet of Things (IoT) networks. Improving EE is especially important for battery limited IoT devices. We observe the uplink and downlink aspects of massive MIMO-OFDM-based IoT networks and categorize some of the effective methods to consider. As uplink aspect, we consider the uplink reference signal (RS) power control. Reducing uplink RS power could induce the battery saving of IoT devices but could cause an increase in channel estimation error. As downlink aspect, we consider the peak-to-average power ratio reduction of the OFDM signal and downlink transmitter power control. These techniques are well-known as effective EE improvement methods, but there is little work showing the actual EE gain in system perspective. In addition, we also consider the utilization of radio frequency energy transfer using unmanned aerial vehicles to extend the operating time of battery-limited IoT devices. We derive the theoretical closed-form approximations of spectral efficiency and EE when applying these methods and provide EE gains for various scenarios. Numerical results show that the theoretical analysis is in good agreement with the simulation results and thus can be used as useful tools to improve EE.

INDEX TERMS Energy efficiency, Internet of Things, massive MIMO-OFDM.

I. INTRODUCTION

Improving energy efficiency (EE) in internet of things (IoT) networks is a vital research topic to deal with. It has been already shown in the literature that massive multiple-input multiple-output (MIMO) systems can be used for IoT networks to improve both spectral efficiency (SE) and EE [1]–[8]. Massive MIMO systems improve the SE of IoT networks by using spatial multiplexing to a large number of distributed IoT devices and/or user equipments (UEs). Moreover, if we increase the number of transmitter (TX) antennas with a limited number of UEs, we can generate a large array gain, which gives us an opportunity to reduce the TX power. The main characteristic of massive MIMO is the channel hardening effect. If the number of service antennas increases with a limited amount of UEs, the channel gain increases while interference and noise are reduced, and the channel gains for all UEs become very similar. It is then very easy to perform channel estimation and interference suppression. One of the main problems in massive MIMO systems is reference signal (RS) overhead that increases as the number of IoT devices and/or UEs increases [9]. Typically, time division duplex (TDD) mode is used for massive MIMO to reduce the RS overhead because in frequency division duplex (FDD) mode, the number of RSs proportionally increases as increasing the number of TX antennas in massive MIMO, and it is very difficult to reduce the large overhead. In TDD mode, the number of RSs increases as the number of UEs increases. However, in general, the number of UEs is smaller than the number of TX antennas in massive MIMO systems.

Orthogonal frequency division multiplexing (OFDM) is a powerful signal transmission method, and it is highly possible that it can be combined with massive MIMO for efficient frequency utilization [10]. However, OFDM signal suffers from a very high peak-to-average power ratio (PAPR), and to cope with this problem, current base stations (BSs) use digital predistortion (DPD) technologies. Since DPD is an expensive device, it cannot be used for massive MIMO due to the burden from the excessive amount of TX antennas [10].

On the other hand, there are several well-known PAPR reduction techniques, and they can be applied in massive MIMO-OFDM [10], [11].

To improve EE, we can observe the massive MIMO-OFDM based IoT networks in two aspects; the downlink aspect and uplink aspect. In the downlink aspect, as mentioned, it is well-known that the PAPR reduction of the massive MIMO-OFDM can be quite important to improve the EE. Due to the high PAPR of the massive MIMO-OFDM signal, high input back-off (IBO) is required, and this causes the reduction of TX radiation power in a given PA power consumption because it reduces the PA efficiency. Iterative clipping and filtering (ICAF) technique can be well applied to massive MIMO-OFDM to increase the PA efficiency, but we must carefully look at the clipping distortion which can reduce the SE, and which can also consequently reduce EE. On the other hand, downlink power control is well suited for increasing the EE of a system because the power consumption of PAs in BS takes more than 50% of total power consumption.

In the uplink aspect, in TDD mode, the quality of the uplink RS significantly affects the accuracy of channel estimation. Increasing uplink RS power increases the channel estimation accuracy. However, to support battery limited IoT devices, the incrasing uplink RS power can reduce the operation time due to the limited battery power maintenance time. Unmanned aerial vehicles (UAVs) and/or drones can be used to provide power to the distributed battery limited IoT devices and extend the battery time [1]. In this paper, the battery time indicates the duration of the operation time of an IoT device before the next required battery charge. The power supply drone can approach the IoT devices and transfer RF energy to charge the battery. RF energy transfer and harvesting techniques have recently become amazing technologies for distributed wireless IoT networks [1], [12]. Transferring energy using an RF signal to the remotely distributed UEs can give significant benefits for the operation of IoT networks. Wireless power transmission generally requires a receiving RF power of at least -20dBm [12], so it is necessary that the drone approaches close to IoT devices. Generally, RF energy transfer is performed using a 300GHz to 3kHz frequency range of electromagnetic radiation. Since the RF power strength is attenuated according to the cube of the reciprocal of distance, only close IoT devices can be directly supported. The drone can move close to the massive MIMO-OFDM data center, receive RF energy from the data center, then move close to the IoT devices that require RF energy, and transfer the RF energy to the IoT devices.

In this paper, we investigate how the uplink RS power control, downlink TX power control, and clipping PAPR reduction schemes can affect the massive MIMO-OFDM system, and provide the EE gains in various scenarios. To this purpose, we derive the closed-form approximations of SE and EE, and provide the performance analysis of the massive MIMO-OFDM based battery limited IoT networks. For the uplink RS power and channel estimation accuracy relation, we assume the channel estimation accuracy increases as uplink RS power increases, whereas the battery time reduces as uplink RS power increases. The uplink RS power can be logically connected to the battery time of IoT devices. Downlink EE increases as required IBO reduces. Required IBO is tightly connected to the PAPR of the OFDM signal. Downlink EE can additionally be increased using downlink TX power control. The EE is defined as SE over power consumption. The power consumption not only includes BS power consumption for downlink signal but also includes UE power consumption for the uplink RS. If we use power supply drones, the power consumption of drones are also included in the total power consumption. Because our work deals with massive MIMO, we use a system model similar to [9] and [10]. Lee [9] has proposed a RS overhead reduction scheme, and Lee and Kim [10] have proposed a clipping PAPR reduction scheme in massive MIMO. This paper deals with the performance gain of various scenarios in high EE massive MIMO.

The main contributions of this paper are shown as follows:

- The closed form equations of SE and EE for various scenarios in massive MIMO-OFDM based battery limited IoT networks are derived. We use the channel estimation error factor to represent the accuracy of channel estimation, and the error factor is a function of uplink RS power. The derived approximations also include the clipping distortion from the clipping PAPR reduction technique. In addition, drone based RF power transfer model is included to extend the battery time of IoT devices.
- Based on the derived SE and EE approximations, we provide SE and EE performance for various scenarios in massive MIMO-OFDM based battery limited IoT networks. There are six cases showing the performance of SE and EE, and each case is summarized in Table 3.

The manuscript is organized as follows: The background and motivation of our work are provided in Section II. The massive MIMO and related system models are described in Section III. The channel model, precoding, clipping PAPR reduction, and power consumption models are discussed in this section. The closed-form approximations of achievable SE and EE are derived in Section IV. Numerical results and related discussions are provided in Section V, and concluding remarks are given in Section VI.

Notation: In the following, the operators $\mathbb{E}[\cdot]$ and $(\cdot)^H$ denote expectation and conjugate transpose, respectively. The $N \times N$ identity matrix is denoted $\mathbf{I}_N$, and the $N \times N$ zero matrix is denoted $\mathbf{0}_N$. $\mathscr{CN}(\mathbf{a}, \mathbf{V})$ is the circular symmetric complex Gaussian distribution with mean $\mathbf{a}$ and covariance $\mathbf{V}$. $\log_2(\cdot)$ denotes the common logarithm. $\circ$ denotes the componentwise product of the matrices. We employ $\mathbf{A}_{i,:}$ to denote the ith row of the matrix $\mathbf{A}$, and $\mathbf{A}_{:,j}$ to denote the jth column of the matrix $\mathbf{A}$. $\|\mathbf{a}\|_\infty$ and $\|\mathbf{a}\|_2$ denote the l_∞-norm, and l_2-norm of vector $\mathbf{a}$, respectively. $\mathbb{C}$ denotes the set of all complex numbers, and $\mathbb{C}^{N \times N}$ denotes the set of all complex $N \times N$ matrices.

II. BACKGROUND AND MOTIVATION

In this section, we provide the background and motivation of this work.

A. BACKGROUND

In view of the fact that the design of an energy efficient wireless system is one of the most important issues in IoT networks, a growing class of researches have been done in recent years. As a MIMO related point of view, Eraslan and Daneshrad [13] presented a low-complexity link adaptation algorithm for maximizing the EE of MIMO-OFDM systems. They proved that the EE is a single-peaked quasi-concave function of the transmit power, and developed an iterative algorithm to find near-optimal transmit power. Through realistic end-to-end bit level simulations, they showed that the complexity of the algorithm is reduced by orders of magnitude while the performance loss is fairly little. Lee [3], Lee and Kim [10], and Lee *et al.* [14] proposed several elegant PAPR reduction schemes to increase the EE of massive MIMO-OFDM systems. Lee [3] proposed a low complexity selected mapping scheme which can be successfully applied to massive MIMO to increase the downlink EE of IoT networks. Lee [3] used a clipping scheme that can increase EE with little performance loss based on the interference awareness. Lee *et al.* [14] proposed a design methodology of the combination of clipping and selected mapping scheme to get even better EE of the system. The proposed schemes can be quite helpful to improve the downlink EE of IoT networks. Lee [15] also showed the EE gain of massive MIMO systems using downlink power control to reduce operation cost and carbon footprint. In addition, a new design paradigm for the high EE operation of massive MIMO BS was presented in [16]. Xu and Qiu [17] proposed a new MIMO EE optimization approach, in which the transmit covariance is optimized under fixed active transmit antenna sets, and then active transmit antenna selection is utilized. During the transmit covariance optimization, they proposed a globally optimal energy efficient iterative water-filling scheme through solving a series of concave-convex fractional programs. Besides, in [18], the method and related performance of non-ideal hardware massive MIMO systems was presented. Authors proved that the huge degrees of freedom offered by massive MIMO can be used to reduce the transmit power and also used to tolerate larger hardware impairments, which allows for the use of inexpensive and energy-efficient antenna elements.

As IoT networks and devices related aspects, there have also been numerous research articles. Zorzi *et al.* [19] presented the current status of the IoT, and discussed how the current situation of many IoT devices should evolve into a much more integrated and heterogeneous system. They also summarized how IoT related challenges can be addressed in order to facilitate the IoT's development. An energy-aware trust derivation scheme using game theoretic approach, which manages overhead while maintaining adequate security of wireless sensor IoT networks was proposed in [20]. Trust evaluation plays an important role in securing wireless IoT sensor networks. In their work, a risk strategy model was presented to stimulate IoT sensor nodes' cooperation. Then, a game theoretic approach was applied to the trust derivation process to reduce the overhead of the process. The scheme aims to minimize the energy consumption and latency of the network under the premise of security assurance. As IoT devices point of view, extending battery operation time is very important. In this regard, Kamalinejad *et al.* [21] presented the enabling technologies for efficient wireless energy harvesting, analyze the lifetime of wireless energy harvesing-enabled IoT devices, and research challenges that lie ahead. The knowledge of channel state information is essential to exploit the energy beamforming gain at the TX. Xu and Zhang [22] a general design framework for a new type of channel learning method based on the receiver's energy measurement feedback. Specifically, the receiver measures the harvested energy levels and sends them to the TX via a feedback link of limited rate. Based on the energy-level feedback, the TX adjusts transmit beamforming and obtains refined estimates of the MIMO channel by convex optimization. Unmaned arial vehicle (UAV) and/or drone could be extensively used for wireless power transfer. Zeng and Zhang [23] studied energy-efficient UAV communication with a ground terminal via optimizing the UAV's trajectory, a new design paradigm that jointly considers both the communication throughput and the UAV's energy consumption. An efficient design was proposed for maximizing the UAV's energy efficiency with general constraints on the trajectory, including its initial/final locations and velocities, as well as minimum/maximum speed and acceleration.

B. MOTIVATION

IoT devices are contiually growing, and the EE improvement of IoT networks is a critical issue [1], [24]–[27]. IoT networks will be applied everywhere, and the importance of industrial IoT network and the application of related cyber-physical systems are also increasing [1]. According to Gartner, the number of connected IoT devices will hit 20.4 billion by 2020.

As we alluded in the previous subsection, massive MIMO-OFDM based IoT network is quite promising, however to enjoy the full benefit of massive MIMO-OFDM, the EE should be carefully considered. The EE is tightly connected with the operation cost, thus without EE improvement, despite its vast SE gain, it is difficult to realize the massive MIMO-OFDM based IoT network. However, there are many degrees of freedom in the massive MIMO-OFDM based IoT networks, therefore we could successfully increase the EE for both downlink and uplink aspects. This can reduce the operation cost and increase the battery time of sensor-like IoT devices, and increase the usability. In this regard, it is very important to carefully examine the EE performance of massive MIMO-OFDM based IoT network in various scenarios. All the previous works we summarized in the previous subsection typically focused on specific technologies, and

little showed the EE gain of the combined technologies. One of the representative previous work is low complexity link adaptation algorithm for maximizing the EE of MIMO-OFDM systems [13]. It is quite effective scheme for power control. On the other hand, we present the EE gain of massive MIMO-OFDM based IoT networks in various scenarios. The system includes uplink/downlink power control, PAPR reduction capabilities. In addition, energy transfer drones for battery limited IoT devices are extensively utilized. The results can be quite useful tools to design the system.

III. SYSTEM MODEL

In this section, we provide IoT and massive MIMO-OFDM related system models. The IoT model, massive MIMO-OFDM, precoding, and power consumption models are presented.

A. IoT MODEL

The block diagram of IoT model we use in this paper is shown in Fig. 1. We consider a single isolated cell with three entities; BS, UE, and UAV.

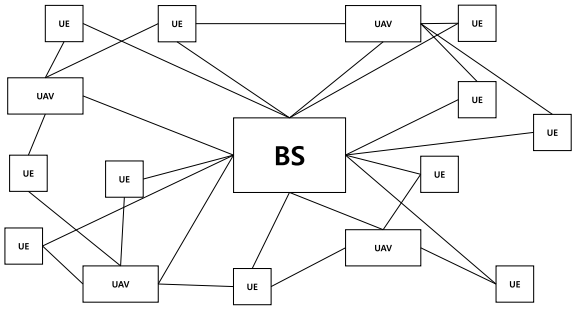

FIGURE 1. Block diagram of IoT network model.

The BS has massive MIMO-OFDM capability with M TX antennas, and deployed at data center. UEs are IoT devices, and the number of UEs is U. Typically U is smaller than M to enjoy the benefit of channel hardening effect. There are another entities, UAV that can transfer energy to the UEs to increase the battery time. The number of UAVs are much smaller than that of UEs. The BS is connected to all UEs and UAVs. Since there are no relays and device-to-device (D2D) connections, the UEs are directly connected to the BS. UAVs are connected to both UEs and BS. There are several UAVs, and thus UAVs only support the UEs near the UAVs. UAVs support all the UEs, so when there are only one UAV, the UAV supports all UEs. M can be adjusted and the range of M is between 50 to 500. Greater M increases SE, but it also increases the power consumption. We can clip the signal to reduce the signal nonlinearity and to improve EE. The TX power also can be adjusted, and the range of downlink TX power is 4 to 40 W. The range of uplink TX power is 100mW to 200mW. Signal carrier frequency is 2GHz. Coherence time and bandwidth is 5 msec and 180kHz respectively. The speed of drone is 10m/sec. More details on the system parameters of IoT model are presented in Section V.

B. MASSIVE MIMO-OFDM MODEL

Now let us consider a single isolated cell with a massive MIMO-OFDM system deployed at data center. Cyclic prefix (CP) is necessary to remove the inter-symbol interference (ISI) due to multipath delay spread. Assuming the CP is longer than the multipath delay spread, the frequency domain representation of the received kth subcarrier signal vector, $\mathbf{Y}[k](= [Y_1[k], Y_2[k], \ldots, Y_U[k]]^T)$, can be represented as follows [10]:

$$\mathbf{Y}[k] = \sqrt{p_{tx}^{dl}}\mathbf{G}[k]\mathbf{X}[k] + \mathbf{N}[k], \tag{1}$$

where $\mathbf{Y}[k]$ is the $U \times 1$ received vector for each UE, p_{tx}^{dl} is the total TX power for a downlink signal, $\mathbf{G}[k]$ is the $U \times M$ channel matrix between M BS antennas and U IoT devices, $\mathbf{X}[k]$ is the $M \times 1$ signal vector for each antenna, and $\mathbf{N}[k]$ is the $U \times 1$ additive white Gaussian noise (AWGN) vector with zero mean and σ_d^2 variance at the IoT devices (i.e., $\mathbf{N}[k] \sim \mathcal{CN}(\mathbf{0}_U, \sigma_d^2\mathbf{I}_U)$). $\mathbf{G}[k]$ consists of both a small scale fading channel matrix, $\mathbf{H}[k]$ and a large scale fading channel matrix, $\mathbf{B}[k]$, i.e., $\mathbf{G}[k] = \mathbf{H}[k] \circ \mathbf{B}[k]$ where $\circ$ indicates the componentwise product. From now on, we omit the subcarrier index, k for simplicity.

C. PRECODING

The precoding process is necessary to reduce the inter-user interference (IUI), when massive MIMO signals are transmitted to many distributed IoT devices. There are two representative linear precoding schemes for massive MIMO: matched filtering (MF) and zero forcing (ZF) schemes [4].

The transmitted signal, $\mathbf{X}$ is represented as follows:

$$\mathbf{X} = \zeta\mathbf{W}\mathbf{S}, \tag{2}$$

$\mathbf{W}$ is the $M \times U$ precoding matrix to reduce the IUI, and ζ is the TX power normalization factor to make the TX signal power as unity. $\mathbf{W} = \mathbf{H}^H$ for MF precoding, and $\mathbf{W} = \mathbf{H}^H(\mathbf{H}\mathbf{H}^H)^{-1}$ for ZF precoding. ζ is approximated as $\zeta_{mf} \approx \frac{1}{\sqrt{MU}}$ for MF precoding and $\zeta_{zf} \approx \sqrt{\frac{M-U}{U}}$ for ZF precoding [28]. $\mathbf{S}$ is the $U \times 1$ message signal vector.

D. POWER CONSUMPTION MODEL

To measure the EE of IoT networks with massive MIMO-OFDM, a tractable power consumption model is necessary. In the BS side, the sum power consumption, $P_{bs,sum}$ can be expressed as:

$$P_{bs,sum} = P_{pa} + M \cdot P_{rf} + P_{bb}, \tag{3}$$

where P_{pa} is the power consumption of the PA, P_{rf} is the RF front-end power consumption of each antenna, and P_{bb} is the baseband power consumption. Due to the beamforming effect, P_{pa} can be decreased as M increases, while the total RF front-end power consumption, $M \cdot P_{rf}$ increases as M increases.

The sum power consumption of UEs, $P_{ue,sum}$ can be expressed in a similar manner:

$$P_{ue,sum} = U \cdot P_{pa}^{ul} + U \cdot P_{rf}^{ul} + U \cdot P_{bb}^{ul}, \tag{4}$$

where P_{pa}^{ul}, P_{rf}^{ul}, and P_{bb}^{ul} are uplink and/or UE side PA power consumption, RF front-end power consumption, and baseband power consumption, respectively. We assume there is no individual power control for each UE. Different from BS side sum power consumption, the power consumption of PA, RF front-end and baseband in the UE side sum power are proportional to the number of IoT devices, U.

To measure the EE based on PA operation, we need to define PA efficiency, η. High η gives low PA power consumption. As an example, the Class-B PA efficiency, $\eta(\%)$, can be shown as [29]–[37]:

$$\eta(\%) = \frac{\pi}{4p_i} \times 100, \tag{5}$$

where p_i is the square-root of IBO, i.e., $\sqrt{IBO}$. IBO is the ratio of the maximum allowable input power or saturation input power of PA, P_{max} and the average power of input signal P_{ave} [36]:

$$IBO(dB) = 10log_{10}\left(\frac{P_{max}}{P_{ave}}\right), \tag{6}$$

Increasing IBO reduces distortion, but also reduces EE. The simple relationship between downlink TX power, p_{tx}^{dl} and P_{pa} can be represented as:

$$p_{tx}^{dl} = \eta_{bs} P_{pa}, \tag{7}$$

where η_{bs} is the PA efficiency of BS.

The relationship between uplink RS power, p_{rs}^{ul} and P_{pa}^{ul} can be represented in a similar manner.

$$p_{rs}^{ul} = \eta_{ue} P_{pa}^{ul}, \tag{8}$$

where η_{ue} is the PA efficiency of UE.

PAPR reduction increases η; thus it can increase p_{tx}^{dl} while maintaining P_{pa}, and/or it can maintain p_{tx}^{dl} with P_{pa} reduction. This fact is reflected in the denominator of EE metric. i.e., if $\eta^p > \eta^w$, then $P_{pa}^p = \frac{P_{tx}^{dl}}{\eta^p} < P_{pa}^w = \frac{P_{tx}^{dl}}{\eta^w}$ where η^p and P_{pa}^p indicate the PA efficiency and PA power consumption with PAPR reduction, and η^w and P_{pa}^w indicate the PA efficiency and PA power consumption without PAPR reduction.

Now we consider the BB power consumption, P_{bb}. BB power consumption is typically much less than PA and RF front-end power consumption. To get the P_{bb}, we use the following floating point operations per second (Gflops), Ψ that was presented in [38]–[40]:

$$\begin{aligned}\Psi(Gflop) &= M \cdot \frac{(T_u B)}{T_s} \cdot \log_2(T_u B) + M \cdot \frac{(T_d B)}{T_{sl}} \cdot \tau_p \cdot \log_2(\tau_p) \\ &\quad + M \cdot U \cdot \left(\frac{T_{sl}}{T_s} \cdot \frac{T_u}{T_d} - \tau_p\right) \cdot \frac{(T_d B)}{T_{sl}} + M \cdot U^2 \cdot \frac{(T_d B)}{T_{sl}},\end{aligned} \tag{9}$$

The description of each parameter is shown in Table 1. We took the parameters from [4] and from a current 3GPP LTE system [41]–[43]. The first part of (9) is to perform the FFT/IFFT operation, the second part is to implement precoding/decoding, the third part is to correlate the RSs with RS sequences, and the last part is to contain the additional pseudo inverse for ZF precoding.

TABLE 1. System parameters.

Parameter	Description	value
B	Bandwidth	$10MHz$
T_{sl}	Slot length	$0.5ms$
T_s	Symbol duration	$71.4us$
T_g	Guard Interval (GI)	$4.7us$
T_u	Symbol without GI	$66.7us$
T_d	Delay spread	$4.7us$

The relationship between P_{bb} and $\Psi(Gflops)$ can be represented as

$$P_{bb}(W) = \frac{\Psi(Gflops)}{\upsilon(Gflops/W)}, \tag{10}$$

where υ is the VLSI processing efficiency, and we use 50 Gflop/W. We assume $T_g = T_d$ for short guard interval and fast RS correlation. When we use MF precoding, the last part of (9) becomes zero, since MF precoding does not need to perform the pseudo inverse [38]–[40].

We should also consider the power consumption of the power supply drone, in case it is used. For steady straight-and-level flight (SLF) of a power supply drone with constant speed V, we have [23]:

$$\bar{E}_{SLF}(V) = T \cdot \left(c_1 \cdot V^3 + \frac{c_2}{V}\right), \tag{11}$$

(11) consists of two terms. The first term, which is proportional to the cubic of the speed V, is known as the parasitic power for overcoming the parasitic drag due to the aircraft's skin friction, form drag, etc. The second term, which is inversely proportional to V, is known as the induced power for overcoming the lift-induced drag, i.e., the resulting drag force due to wings redirecting air to generate the lift for compensating for the aircraft's weight. Based on (11), the power consumption for one drone can be represented as:

$$P_{drone} = \frac{\bar{E}_{SLF}(V)}{T} = \left(c_1 \cdot V^3 + \frac{c_2}{V}\right). \tag{12}$$

The power consumption of (11) as a function of V is illustrated in Fig. 2. We use $c_1 = 9.26 \times 10^{-4}$ and $c_2 = 2250$ as shown in [23]. According to Fig. 2, the minimum P_{drone} becomes 100.002W, when $V = 29.9994$ m/s.

We model the total power consumption of a power supply drone, P_{drone}^{tot} as follows:

$$P_{drone}^{tot} = \Lambda \cdot \left(\frac{p_{rs}^{ul}}{p_{rs,max}^{ul}}\right) \cdot P_{drone}. \tag{13}$$

where Λ is the number of required drones, p_{rs}^{ul} and $p_{rs,max}^{ul}$ are the uplink RS power and maximum uplink RS power of UEs respectively. As the RS power of the UE increases, P_{drone}^{tot} increases. This is logically true, because increasing UE RS power reduces battery operating time, and thus the power supply drones must move more often to supply the power. In real situation, an appropriate adjustable factor can be multiplied to

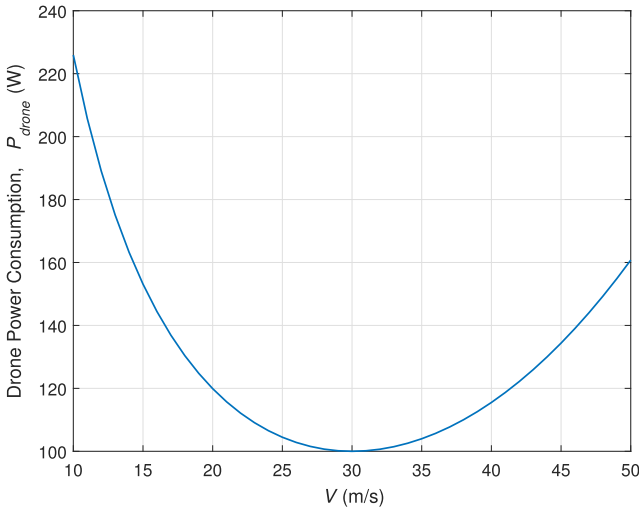

FIGURE 2. Drone power consumption versus speed of drone.

smoothing the model in (13). As mentioned, we use wireless power transfer using sub-6GHz RF signal. Drones can very closely approach to the IoT devices, thus the efficiency of the RF energy transfer can be high. In practice, the RF related energy is much smaller than the drone propulsion energy, and thus is ignored [23].

IV. CLOSED-FORM APPROXIMATIONS OF ACHIEVABLE SPECTRAL EFFICIENCY AND ENERGY EFFICIENCY

In this section, we derive the closed-form equations of achievable SE and EE with channel estimation error and PAPR reduction.

A. SPECTRAL EFFICIENCY

To get the SE, first we model the estimated channel, $\hat{\mathbf{H}}$, as follows [8]:

$$\hat{\mathbf{H}} = \xi\mathbf{H} + \sqrt{1-\xi^2}\mathbf{E}, \tag{14}$$

where $\xi \in [0\,,\ 1]$ is the error factor, which reflects the degree of channel estimation error, and $\mathbf{E} \in \mathbb{C}^{U\times M}$ is the error matrix with the same statistical characteristics but independent of the channel, $\mathbf{H}$. The accuracy of the channel estimation heavily depends on uplink RS power. Boosting uplink RS power increases the accuracy of channel estimation, but it requires more power consumption, and possibly reduces the EE. To provide the seriousness of channel estimation error due to the uplink power control, we model ξ as follows:

$$\xi = \kappa\left(\frac{p_{rs}^{ul}}{p_{rs,max}^{ul}}\right)^{1/8}, \tag{15}$$

where κ is the channel estimation error regardless of uplink RS power, and $p_{rs,max}^{ul}$ is the maximum allowable TX power for an uplink RS signal.

The $U \times M$ channel matrix, $\mathbf{G}$ can be shown as,

$$\mathbf{G} = \begin{pmatrix} G_{1,1} & G_{1,2} & \cdots & G_{1,M} \\ G_{2,1} & G_{2,2} & \cdots & G_{2,M} \\ \vdots & \vdots & \vdots & \vdots \\ G_{U,1} & G_{U,2} & \cdots & G_{U,M} \end{pmatrix} = \begin{pmatrix} \mathbf{G}_{1,:} \\ \mathbf{G}_{2,:} \\ \vdots \\ \mathbf{G}_{U,:} \end{pmatrix}, \tag{16}$$

where $\mathbf{G}_{i,:}$ is the $1 \times M$ channel vector for the ith IoT device.

The $M \times U$ precoding matrix, $\mathbf{W}$ can be represented as,

$$\mathbf{W} = \begin{pmatrix} W_{1,1} & W_{1,2} & \cdots & W_{1,U} \\ W_{2,1} & W_{2,2} & \cdots & W_{2,U} \\ \vdots & \vdots & \vdots & \vdots \\ W_{M,1} & W_{M,2} & \cdots & W_{M,U} \end{pmatrix} = \begin{pmatrix} \mathbf{W}_{:,1} & \mathbf{W}_{:,2} & \cdots & \mathbf{W}_{:,U} \end{pmatrix}, \tag{17}$$

where $\mathbf{W}_{:,i}$ is the $M \times 1$ channel vector for the ith IoT device. The effective channel at the receiver after precoding, $\mathbf{G}\cdot\mathbf{W}$ can then be represented as,

$$\mathbf{G}\cdot\mathbf{W} = \begin{pmatrix} \mathbf{G}_{1,:} \\ \mathbf{G}_{2,:} \\ \vdots \\ \mathbf{G}_{U,:} \end{pmatrix} \cdot \begin{pmatrix} \mathbf{W}_{:,1} & \mathbf{W}_{:,2} & \cdots & \mathbf{W}_{:,U} \end{pmatrix} = \begin{pmatrix} \mathbf{G}_{1,:}\cdot\mathbf{W}_{:,1} & \mathbf{G}_{1,:}\cdot\mathbf{W}_{:,2} & \cdots & \mathbf{G}_{1,:}\cdot\mathbf{W}_{:,U} \\ \mathbf{G}_{2,:}\cdot\mathbf{W}_{:,1} & \mathbf{G}_{2,:}\cdot\mathbf{W}_{:,2} & \cdots & \mathbf{G}_{2,:}\cdot\mathbf{W}_{:,U} \\ \vdots & \vdots & \vdots & \vdots \\ \mathbf{G}_{U,:}\cdot\mathbf{W}_{:,1} & \mathbf{G}_{U,:}\cdot\mathbf{W}_{:,2} & \cdots & \mathbf{G}_{U,:}\cdot\mathbf{W}_{:,U} \end{pmatrix}, \tag{18}$$

The symbol received by the uth IoT device can be given by

$$Y_u = \sqrt{p_{tx}^{dl}}\zeta\left(\mathbf{H}_{u,:}\circ\mathbf{B}_{u,:}\right)\mathbf{W}_{:,u}S_u + N_u + \sqrt{p_{tx}^{dl}}\zeta\sum_{l\neq u}\left(\mathbf{H}_{u,:}\circ\mathbf{B}_{u,:}\right)\mathbf{W}_{:,l}S_l, \tag{19}$$

where $\mathbf{H}_{u,:}$ and $\mathbf{B}_{u,:}$ are the $1 \times M$ small scale and large scale channel vectors for the uth IoT device respectively, N_u is the AWGN for the uth IoT device, and $\mathbf{W}_{:,u}$ is the $M \times 1$ precoding vector for the uth IoT device. The last term of (19) is the IUI. Assuming all the path loss components from BS to uth IoT device are the same, the effective SINR at the receiver (RX) for the uth IoT device, γ_u, can be represented as follows:

$$\gamma_u = \frac{\rho_r|\zeta\mathbf{H}_{u,:}\mathbf{W}_{:,u}|^2}{\rho_r\sum_{l\neq u}|\zeta\mathbf{H}_{u,:}\mathbf{W}_{:,l}|^2+1}, \tag{20}$$

where $\rho_r = \frac{p_{tx}^{dl}\cdot\beta_u}{N_0\,B}$ is the received signal-to-noise ratio (SNR) at RX, β_u is the path loss component between BS and the uth IoT device, and $N_0\,B$ is the noise power in the given bandwidth, B.

The downlink SE can be represented as:

$$R^d = \Theta \sum_{i=1}^{\chi^d} \varsigma^d \left(1 - \frac{\tau_p}{\tau_c}\right) \log_2(1+\gamma_i). \quad (21)$$

where χ^d are the adjustable factors to reflect the number of coincidently supported IoT devices for downlink transmission and typical value of χ^d is U when $U < M$, and ς^d is the parameter to reflect the actual data transmission resource slot for downlink, i.e., $\varsigma^u + \varsigma^d = 1$ where ς^u is the parameter to reflect the actual data transmission resource slot for uplink. In this paper, we assume that half of the data transmission portion is dedicated to the uplink data transmission, i.e., $\varsigma^u = \varsigma^d = 0.5$. τ_p is the number of resource elements for RS, and τ_c is the number of resource elements in coherence time. Θ is the battery operation time which can be represented as:

$$\Theta = \left(1 - \frac{p_{rs}^{ul}}{p_{rs,\max}^{ul}}\right) + 0.5, \quad 0.5 p_{rs,\max}^{ul} \le p_{tx}^{ul} \le p_{rs,\max}^{ul}, \quad (22)$$

From now on, we derive the SINR for the ith IoT device, γ_i for various cases.

1) SINR WITHOUT DISTORTION

First, we show the reference SINR based on MF precoding. The reference SINR indicates the SINR without any distortion and loss. By using channel hardening effect of the massive MIMO systems [4], the reference SINR based on MF precoding, γ_{mf}^{ref}, can be simplified as follows [8], [9]:

$$\gamma_{u,mf}^{ref} = \frac{\rho_r |\zeta_{mf} \mathbf{H}_{u,:} \mathbf{H}_{u,:}^H|^2}{\rho_r \sum_{l \ne u} |\zeta_{mf} \mathbf{H}_{u,:} \mathbf{H}_{l,:}^H|^2 + 1} \approx \frac{M}{U} \left(\frac{\rho_r}{\rho_r + 1}\right). \quad (23)$$

The reference SINR based on ZF precoding, $\gamma_{u,zf}^{ref}$, can be derived in a similar manner [8].

$$\gamma_{u,zf}^{ref} \approx \frac{M-U}{U} (\rho_r). \quad (24)$$

2) SINR WITH CHANNEL ESTIMATION ERROR

Uplink TX power can be controlled to improve the EE. We should remember that a lot of IoT devices are battery limited sensor devices. In this situation, if we use full TX power for uplink RS, the battery charging time could be required for the battery limited IoT devices. The battery maintenance time of sensor devices largely depends on the uplink TX power because the uplink TX power consumes most of the operation power for sensor devices. If we reduce the uplink RS power, we can secure more operation time; however this causes channel estimation error. If there is a channel estimation error for any reason, the effective SINR based on MF precoding can be expressed as follows:

$$\hat{\gamma}_{u,mf} = \frac{\rho_r \left|\zeta_{mf} \mathbf{H}_{u,:} \hat{\mathbf{H}}_{u,:}^H\right|^2}{\rho_r \sum_{l \ne u} \left|\zeta_{mf} \mathbf{H}_{u,:} \hat{\mathbf{H}}_{l,:}^H\right|^2 + 1}, \quad (25)$$

where $\hat{\mathbf{H}}_{u,:}$ is the $1 \times M$ estimated channel vector for the uth IoT device. Using (14) and statistical approximation, (25) can be simplified as follows:

$$\hat{\gamma}_{u,mf} = \frac{\rho_r \left|\zeta_{mf} \xi \mathbf{H}_{u,:} \mathbf{H}_{u,:}^H + \zeta_{mf} \sqrt{1-\xi^2} \mathbf{H}_{u,:} \mathbf{E}_{u,:}^H\right|^2}{\rho_r \sum_{l \ne u} \left|\zeta_{mf} \xi \mathbf{H}_{u,:} \mathbf{H}_{l,:}^H + \zeta_{mf} \sqrt{1-\xi^2} \mathbf{H}_{u,:} \mathbf{E}_{l,:}^H\right|^2 + 1},$$
$$\approx \frac{M}{U} \left(\frac{\xi^2 \rho_r}{\rho_r + 1}\right). \quad (26)$$

where $\mathbf{E}_{l,:}$ is the $1 \times M$ channel estimation error vector.

Using (14) and statistical approximation, the effective SINR based on ZF precoding with channel estimation error can be derived as follows [44]:

$$\hat{\gamma}_{u,zf} \approx \frac{M-U}{U} \left(\frac{\xi^2 \rho_r}{(1-\xi^2)\rho_r + 1}\right). \quad (27)$$

In a real situation, p_{rs}^{ul} increment guarantees ξ increment. However, increasing p_{rs}^{ul} may not always be beneficial, because it causes battery operation time reduction.

3) SINR WITH CLIPPING DISTORTION

Now, we consider the SINR when the ICAF PAPR reduction technique is applied. It is easy to show the analysis in frequency domain. Based on the result in [10], the clipped massive MIMO-OFDM TX signal in the frequency domain, $\widehat{X}_t$, is the combination of message signals, $S_l, l = 1, 2, \cdots, U$ and elements of the precoding matrix, $W_{t,l}, l = 1, 2, \cdots, U$, and the relationship can be represented as:

$$\widehat{X}_t = \alpha_t \sum_{l=1}^{U} \zeta W_{t,l} S_l + \delta \tilde{D'}_t, \quad (28)$$

where $\tilde{D'}_t$ is the frequency domain clipping distortion noise in a given band, and δ is the adjustment factor due to the precoding and normalization.

Based on (18), after compensating α_t, the symbol received by the uth IoT device is given by,

$$Y_u = \sqrt{p_{tx}^{dl}} \zeta \mathbf{G}_{u,:} \mathbf{W}_{:,u} S_u + \sqrt{p_{tx}^{dl}} \zeta \sum_{l \ne u} \mathbf{G}_{u,:} \mathbf{W}_{:,u} S_l$$
$$+ \sqrt{p_{tx}^{dl}} \delta \mathbf{G}_{u,:} \mathbf{D} + N_u, \quad (29)$$

where $\mathbf{D}(= [\tilde{D'}_1, \tilde{D'}_2, \cdots, \tilde{D'}_M]^T)$ is the $M \times 1$ clipping distortion vector, and N_u is the AWGN for the ith IoT device. From (29), the effective SINR, $\hat{\gamma}_u^c$, can be represented as follows:

$$\hat{\gamma}_u^c = \frac{\rho_r |\zeta \mathbf{H}_{u,:} \mathbf{W}_{:,u}|^2}{\rho_r \sum_{l \ne u} |\zeta \mathbf{H}_{u,:} \mathbf{W}_{:,l}|^2 + \rho_r |\delta \mathbf{H}_{u,:} \mathbf{D}|^2 + 1}. \quad (30)$$

Note that the large scale fading effect is reflected in ρ_r. $\mathbf{H}_{i,:}$ has zero mean and unit variance i.i.d. Rayleigh distribution characteristic, and is independent with $\mathbf{D}$. Based on the Parseval's theorem, the clipping distortion for the ith antenna $\tilde{D'}_i$ can be approximated as [10]:

$$\tilde{D'}_i = \psi \left(e^{-v^2} - \sqrt{\pi} v \cdot erfc(v)\right), \quad (31)$$

where ψ is the adjustable factor of the ICAF distortion power. When we apply 4 times oversampling and 5 iterations, we use $\psi = 3.85$ from $\nu = 0$ dB to 3 dB, and use $\psi = 2.85$ for the rest of ν, and it is in good agreement with real nonlinear ICAF result. Without oversampling and iterations, we use $\psi = 1$, and it is exactly matched with the simulation result, however this case is not applicable for real systems. The clipping process is generally performed after precoding, and the clipping distortion noise also increases as M increases.

Based on the analysis in this subsection and previous subsection, using (26), (27), (30) and (31), the SINR of MF and ZF precoding with channel estimation error and clipping distortion noise can be approximated as in (32) and (33) shown at the bottom of the page.

B. ENERGY EFFICIENCY

EE has become important metric to deal with. EE can be represented as bps per Watt and defined as follows:

$$EE = \frac{B \cdot R^d}{P_{sum}}, \tag{34}$$

Based on the analysis in section III-D, the sum power, P_{sum} can be represented as:

$$P_{sum} = \left(\frac{\tau^{dl}_{data} + \tau^{dl}_{p}}{\tau_c}\right) \cdot \left(P_{pa} + M \cdot P_{rf} + P_{bb}\right) + \left(\frac{\tau_p}{\tau_c}\right) \cdot \left(U \cdot P^{ul}_{pa} + U \cdot P^{ul}_{rf} + U \cdot P^{ul}_{bb}\right) + P^{tot}_{drone}, \tag{35}$$

where τ^{dl}_{data} and τ^{dl}_{p} is the time duration for downlink data transmission and downlink RS respectively. Then, using (32), (33), and (35), the EE of MF and ZF precoded massive MIMO-OFDM applied to IoT networks can be represented as in (36) and (37) shown at the bottom of the next page.

We will validate the closed-form approximations using simulations in the following section.

V. NUMERICAL RESULTS AND DISCUSSION

In this section, we provide the numerical results to show the EE gain of various cases using the closed-form approximations we derived in the previous section, and extensive monte-carlo (MC) simulations. The simulation parameters we use in this section are presented in Table 2.

We use the coherence time, $T_c = 5$ msec, coherence bandwidth, $B_c = 180$kHz, and one RS is dedicated to each IoT device. If we consider a 3GPP based system, 5 msec of time duration generally corresponds to 70 symbols at 15kHz bandwidth, and it can support nomadic and/or relatively slow speed IoT devices [41]–[43]. The size of one resource element is 15kHz $\times$ 71.4usec. The total resource elements in one coherence time is 840 ($12 \times 14 \times 5$). We use a 10MHz signal bandwidth, and 40W maximum downlink data signal TX power which also corresponds to the 3GPP based system. The RF front-end power of the BS and IoT device is 0.5W and 0.1W, respectively. Downlink TX power is controlled to increase EE. The maximum uplink RS power is 200mW, which is almost the same as the typical mobile terminals. Uplink RS power is controlled to increase EE, and if uplink RS power is reduced, the channel estimation error becomes more serious. We use the ETSI path loss model with carrier frequency, $f_c = 2$ GHz [45]. The number of TX antennas, M for massive MIMO-OFDM system deployed at a data center is from 50 to 500, and the number of IoT devices is 10% of M to enable the benefits of the channel hardening effect. We assume the number of uplink RS is the same as the number of UEs, and the number of downlink RS can be negligible due to the channel hardening effect. We use various clipping ratios for the ICAF PAPR reduction technique to increase EE. We choose the speed of power supply drone, V as 10 m/s to cover the industrial IoT networks. This is not the speed needed for the minimum power consumption, which is 29.9994 m/s. To cover various scenarios, we should also consider the case of industrial IoT (IIoT) networks. In IIoT networks, the required coverage of smart factories could be smaller than several dozens of meters, and there could be many objects and/or obstacles to avoid. Thus we reduce the speed of the drone to 10 m/s for practical usage scenarios, even though the power consumption of the drone becomes more than twice the minimum power consumption level.

TABLE 2. Simulation parameters.

Parameter	Value
Coherence Time, T_c	5 msec
Coherence Bandwidth, B_c	180kHz
Total symbols in coherence interval, S_{tot}	840
Signal Bandwidth, B	10 MHz
Downlink data signal TX power, p^{dl}_{tx}	4 $\sim$ 40 W
Uplink RS power, p^{ul}_{rs}	100mW $\sim$ 200mW
Carrier Frequency, f_c	2 GHz
Path Loss Model	ETSI
Number of TX antennas, M	50 $\sim$ 500
Clipping Ratio, ν	1 $\sim$ 10 dB
Speed of drone, V	10 m/sec
Precoding	ZF, MF

$$\hat{\gamma}^c_{u,mf} \approx \frac{M}{U}\left(\frac{\xi^2\rho_r}{\rho_r + \xi^2\rho_r\left(\frac{M}{U}\right)\psi\left(e^{-v^2} - \sqrt{\pi}v \cdot erfc(v)\right) + 1}\right) \tag{32}$$

$$\hat{\gamma}^c_{u,zf} \approx \frac{M-U}{U}\left(\frac{\xi^2\rho_r}{(1-\xi^2)\rho_r + \xi^2\rho_r\left(\frac{M-U}{U}\right)\psi\left(e^{-v^2} - \sqrt{\pi}v \cdot erfc(v)\right) + 1}\right) \tag{33}$$

TABLE 3. Cases for numerical analysis.

Cases	Description
Case I	$p_{rs}^{ul} = 200$mW, Powered IoT devices, clipping PAPR reduction technique with $\nu = 0 \sim 10$ dB.
Case II	$p_{rs}^{ul} = 100$mW, Powered IoT devices, clipping PAPR reduction technique with $\nu = 0 \sim 10$ dB.
Case III	Powered IoT devices, uplink RS power control, $p_{rs}^{ul} = 100 \sim 200$mW.
Case IV	Battery-Limited IoT devices, uplink RS power control, $p_{rs}^{ul} = 100 \sim 200$mW.
Case V	(a) $p_{rs}^{ul} = 200$mW, Battery-Limited IoT devices with three drones (b) $p_{rs}^{ul} = 200$mW, Battery-Limited IoT devices with five drones
Case VI	$p_{rs}^{ul} = 100$mW, Battery-Limited IoT devices with one drone

Since there are a lot of parameters that can adjust EE, various cases can be applied to observe the EE gains. We observe 6 cases which are summarized in Table 3.

We apply the clipping PAPR reduction technique to improve EE for Case I and Case II. Case I is where $p_{rs}^{ul} = 200$mW with powered IoT devices. This case is one of the most desirable cases in the EE perspective, because we can use full TX power for uplink RS due to the power-line to the IoT devices. There is little channel estimation error, and thus there is little SE loss. Power supply drones are not necessary. However, this case is not a general case for battery-limited IoT devices. There are several obstacles to using powered IoT devices. Using powered IoT devices are expensive to install, and the powered IoT devices cannot be applied to moving IoT devices. Case II is where uplink RS power, p_{rs}^{ul} is reduced to 100mW with powered IoT devices. If a kind of sensor device is used, uplink TX power consumes most of the operation power for the device, thus reducing p_{rs}^{ul} can be very helpful to improve EE.

We apply the uplink RS power control to improve EE in Case III and Case IV. Case III deals with serving powered IoT devices, and Case IV deals with serving battery-limited IoT devices. There needs to be an interval for charging the battery in Case IV, and during the interval, we assume the transmission / reception is stopped.

We apply downlink power control to improve EE for Case V and Case VI. Downlink power control is a very effective scheme to improve EE. For Cases V and VI, we only serve battery-limited IoT devices because it is a more common case for distributed IoT devices. Instead of a battery charging interval, we use power supply drones which we presented in sections III-D and IV-B. Case V shows the case when p_{rs}^{ul} is 200mW. In this case, more drones are necessary to support the distributed IoT devices, because battery duration time is shorter than the case of $p_{rs}^{ul} = 100$mW. Thus, in Case V-(a), we assume we use three drones, and in Case V-(b), we assume we use five drones. Case VI shows the case when p_{rs}^{ul} is 100mW. Since battery time can be longer than $p_{rs}^{ul} = 200$mW, we assume we only use one drone.

Remark 1: ICAF is a practical PAPR reduction technique to use for massive MIMO based IoT networks, but clipping ratio should be carefully chosen because high clipping ratio reduces SE, and it causes EE loss.

Fig. 3 shows SE (bps/Hz) versus number of TX antennas, M, when ZF precoding and the ICAF PAPR reduction technique are applied. Red '*'s indicate the simulation results and lines indicate the derived closed-form approximations from (21), (32), and (33) with $\xi = 1$. As observed, the closed-form approximations are well-matched with the simulation results.

Fig. 4 shows SE (bps/Hz) versus number of TX antennas, M, when MF precoding and ICAF PAPR reduction technique are applied. The SE of ZF precoding shows much better performance than that of MF precoding. Due to the clipping distortion, as ν decreases, SE decreases. MF precoding has higher robustness than ZF precoding for clipping distortion. $\nu = 5$ dB is allowable for MF precoding, while values higher than $\nu = 7$ dB should be applied to ZF precoding to maintain little SE loss. This is because, in the case of MF precoding, IUI is already dominant, and if clipping distortion is smaller than IUI, there is little SE performance loss.

$$EE_{mf} = \frac{B \cdot \Theta \cdot \sum_{i=1}^{\chi^d} \varsigma^d \left(1 - \left(\frac{\tau_p + \tau_p^{dl}}{\tau_c}\right)\right) \log_2 \left(1 + \frac{M}{U} \left(\frac{\xi^2 \rho_r}{\rho_r + \xi^2 \rho_r \left(\frac{M}{U}\right) \psi \left(e^{-\nu^2} - \sqrt{\pi}\nu \cdot erfc(\nu)\right) + 1}\right)\right)}{\left(\frac{\tau_{data}^{dl} + \tau_p^{dl}}{\tau_c}\right) \cdot \left(P_{pa} + M \cdot P_{rf} + P_{bb}\right) + \left(\frac{\tau_p}{\tau_c}\right) \cdot \left(U \cdot P_{pa}^{ul} + U \cdot P_{rf}^{ul} + U \cdot P_{bb}^{ul}\right) + P_{drone}^{tot}} \tag{36}$$

$$EE_{zf} = \frac{B \cdot \Theta \cdot \sum_{i=1}^{\chi^d} \varsigma^d \left(1 - \left(\frac{\tau_p + \tau_p^{dl}}{\tau_c}\right)\right) \log_2 \left(1 + \frac{M-U}{U} \left(\frac{\xi^2 \rho_r}{(1-\xi^2)\rho_r + \xi^2 \rho_r \left(\frac{M-U}{U}\right) \psi \left(e^{-\nu^2} - \sqrt{\pi}\nu \cdot erfc(\nu)\right) + 1}\right)\right)}{\left(\frac{\tau_{data}^{dl} + \tau_p^{dl}}{\tau_c}\right) \cdot \left(P_{pa} + M \cdot P_{rf} + P_{bb}\right) + \left(\frac{\tau_p}{\tau_c}\right) \cdot \left(U \cdot P_{pa}^{ul} + U \cdot P_{rf}^{ul} + U \cdot P_{bb}^{ul}\right) + P_{drone}^{tot}} \tag{37}$$

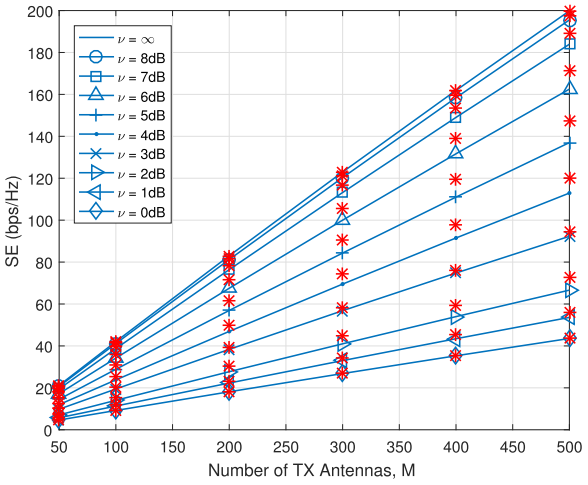

FIGURE 3. SE (bps/Hz) versus number of TX antennas, M, when ZF precoding and ICAF PAPR reduction technique are applied.

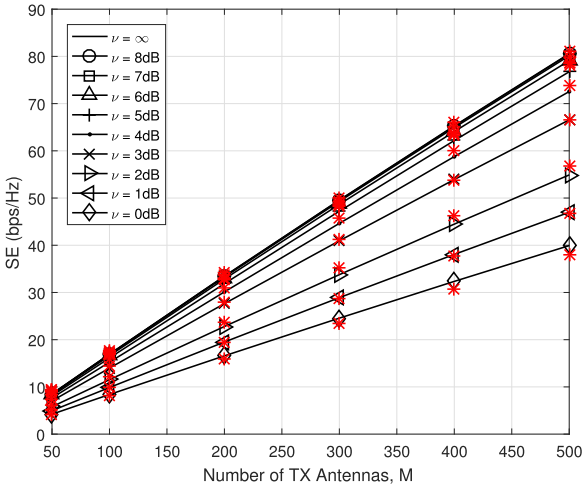

FIGURE 4. SE (bps/Hz) versus number of TX antennas, M, when MF precoding and ICAF PAPR reduction technique are applied.

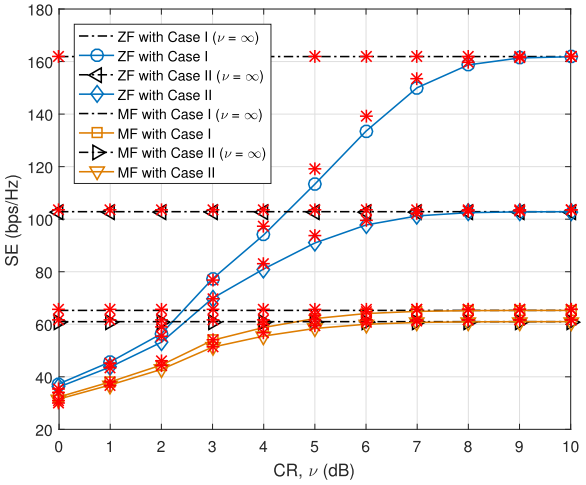

FIGURE 5. SE (bps/Hz) versus clipping ratio, ν, when ZF and MF precodings are applied in the Case I and Case II, $M = 400$, $K = 40$.

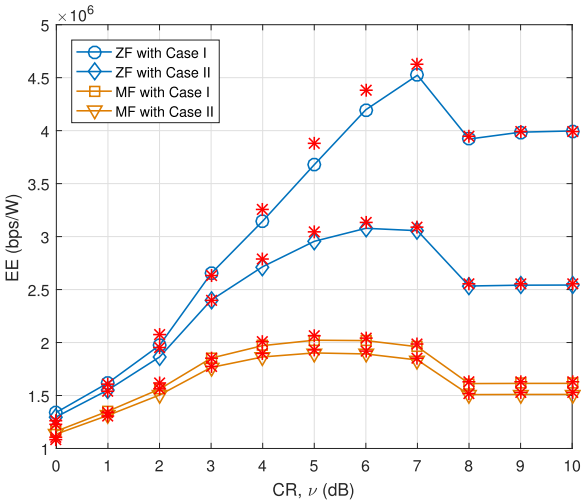

FIGURE 6. EE (bps/W) versus clipping ratio, ν, when ZF and MF precodings are applied in Case I and Case II, $M = 400$, $K = 40$.

Remark 2: For optimum EE, clipping ratio should be chosen as 7dB for ZF precoding, and 5dB for MF precoding. MF precoding is more robust than ZF precoding to clipping noise.

Remark 3: ICAF technique gives better performance gain when uplink RS power is small and MF precoding is used.

Fig. 5 shows SE (bps/Hz) versus clipping ratio, ν, when ZF and MF precodings are applied in Case I and Case II. Black dotted parallel lines are reference lines without any clipping distortion, i,e. $\nu = \infty$. When ZF precoding is applied, Case I shows much better SE than Case II. Due to the low uplink RS power, the performance of Case II has decreased by 36.47% (161.9 $\rightarrow$ 102.85 bps/Hz) at $\nu = 10$dB. When MF precoding is applied, the performance loss due to uplink RS power reduction is only 6.58% (65.3 $\rightarrow$ 61.0 bps/Hz) at $\nu = 10$dB. In addition, we can observe that, to get little SE performance loss while using the clipping PAPR reduction technique, ν should be higher than 7 dB for ZF precoding, and 5 dB for MF precoding. Overall, MF precoding has much higher robustness than ZF precoding for clipping distortion.

Fig. 6 shows EE (bps/W) versus clipping ratio, ν, when ZF and MF precoding are applied in Case I and Case II. EE increases up to $\nu = 7$dB for ZF precoding and increases up to $\nu = 5$dB for MF precoding, then decreases. In our simulation setup, it is shown that $\nu = 7$dB and $\nu = 5$dB are optimum EE choices for ZF and MF precodings, respectively. With ZF precoding, Case I shows 6.25% EE improvement (4 $\rightarrow$ 4.25 (Mbps/W)), while Case II shows 20.47% EE improvement (2.54 $\rightarrow$ 3.06 (Mbps/W)) compared with $\nu = \infty$. With MF precoding, Case I shows 25.47% EE improvement (1.61 $\rightarrow$ 2.02 (Mbps/W)), while Case II shows 25.83% EE improvement (1.51 $\rightarrow$ 1.9 (Mbps/W)) compared with $\nu = \infty$. Case II shows better EE improvement for both ZF and MF precoding. However, with ZF precoding,

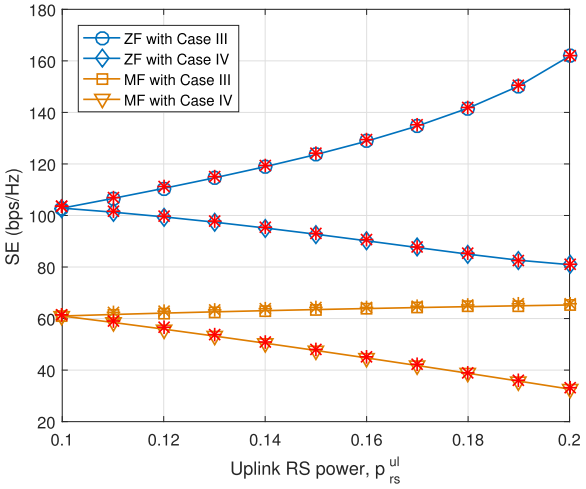

FIGURE 7. SE (bps/Hz) versus uplink RS power, p_{rs}^{ul}, when ZF and MF precodings are applied in Case III and Case IV, $M = 400, K = 40$.

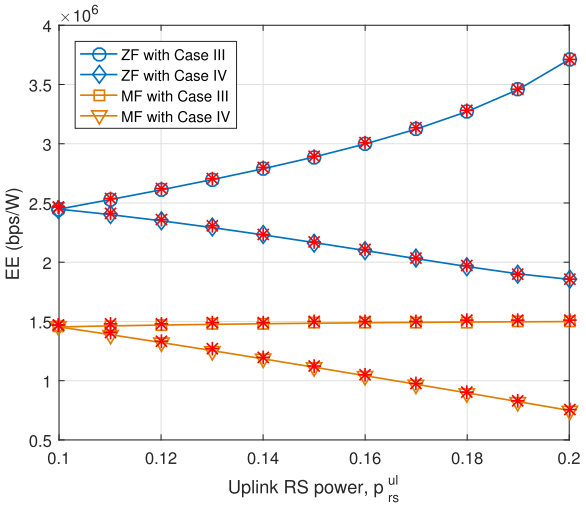

FIGURE 8. EE (bps/W) versus uplink RS power, p_{rs}^{ul}, when ZF and MF precodings are applied in Case III and Case IV, $M = 400, K = 40$.

the difference is large, whereas with MF precoding, there is little difference between Case I and Case II.

Remark 4: With ZF precoding, increasing uplink RS power is beneficial to EE improvement for powered IoT devices, while reducing uplink RS power is helpful for battery-limited IoT devices. With MF precoding, controlling uplink RS power helps little to EE improvement for powered IoT devices, while reducing uplink RS power is helpful for battery-limited IoT devices.

Fig. 7 shows SE (bps/Hz) versus uplink RS power, p_{rs}^{ul}, when ZF and MF precodings are applied in Case III and Case IV. In Case III, as p_{rs}^{ul} increases, SE increases. However, in Case IV, as p_{rs}^{ul} increases, SE decreases. This is because, as p_{rs}^{ul} increases, battery charging time also increases which results in the decrease of SE. In this paper, as we mentioned, we assume signal transmission/reception is stopped during battery charging time. If not, the SE of battery limited IoT devices is the same as that of powered IoT devices which is not fair for the system comparison point of view.

The reduction of p_{rs}^{ul} could help to improve EE. Fig. 8 shows EE (bps/W) versus uplink RS power, p_{rs}^{ul}, when ZF and MF precodings are applied in Case III and Case IV. As observed, uplink RS power control little help to improve EE in Case III. This is due to the fact that the SE loss from channel estimation error is higher than the power saving from the reduction of p_{rs}^{ul}. Even though p_{rs}^{ul} takes a large portion of the power consumption in sensor devices, SE loss is more critical due to the reduction of p_{rs}^{ul}. Thus, maximum p_{rs}^{ul} for RS is helpful to improve EE in Case III. This result is the same as the case of cellular networks. Boosting RS power is beneficial when there is no interference. However, uplink RS power control provides relatively high benefit in Case IV with ZF precoding. This comes from the saving of battery charging time in battery limited IoT devices. The similar characteristic can be observed for MF precoding. With ZF precoding, Case III shows 51.43% EE improvement

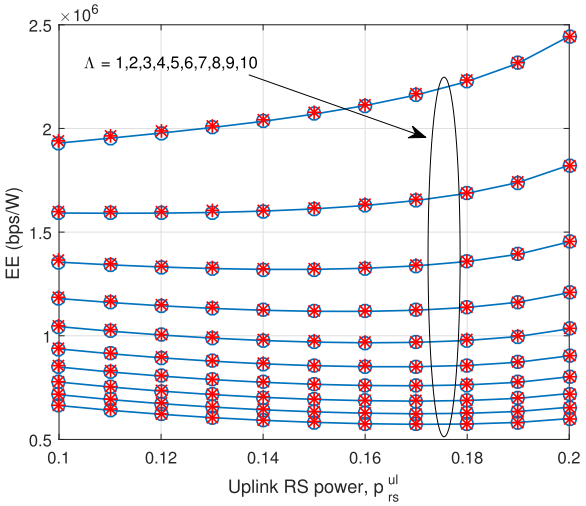

FIGURE 9. EE (bps/W) versus uplink RS power, p_{rs}^{ul}, when ZF precoding is applied, $M = 400, K = 40$.

(2.45 → 3.71 (Mbps/W)), while Case IV shows 31.72% EE improvement (1.86 → 2.45 (Mbps/W)) from p_{rs}^{ul} = 100mW to p_{rs}^{ul} = 200mW. With MF precoding, Case III shows 3.45% EE improvement (1.45 → 1.5 (Mbps/W)) from p_{rs}^{ul} = 100mW to p_{rs}^{ul} = 200mW, while Case IV shows 93.33% EE improvement (0.75 → 1.45 (Mbps/W)) from p_{rs}^{ul} = 200mW to p_{rs}^{ul} = 100mW. In case III, there is little EE improvement using uplink RS power control with MF precoding.

Remark 5: With ZF precoding, when the number of required drones, Λ is small, increasing uplink RS power improves EE. On the other hand, as the number of required drones, Λ increases, adjusting uplink RS power gives little performance variation.

A power supply drone is necessary to charge the batteries of distributed IoT devices. Fig. 9 shows the EE (bps/W)

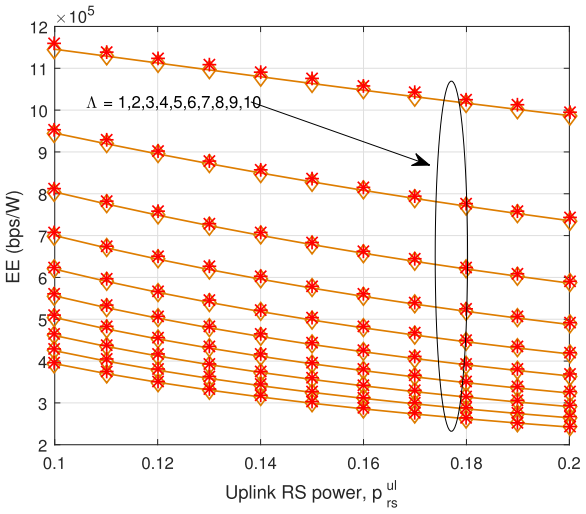

FIGURE 10. EE (bps/W) versus uplink RS power, p_{rs}^{ul}, when MF precoding is applied, $M = 400, K = 40$.

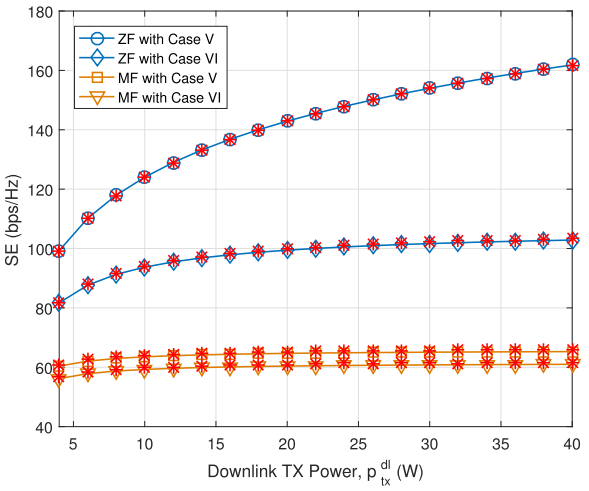

FIGURE 11. SE (bps/Hz) versus downlink TX power, p_{tx}^{dl}, when ZF and MF precodings are applied in Case V and VI, $M = 400, K = 40$.

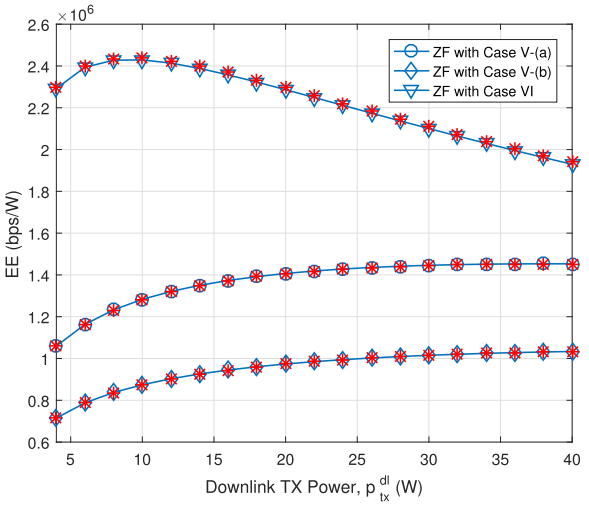

FIGURE 12. EE (bps/W) versus downlink TX power, p_{tx}^{dl}, when ZF precoding is applied in Case V and VI, $M = 400, K = 40$.

versus uplink RS power, p_{rs}^{ul}, when ZF precoding is applied. When the number of required drones Λ is small, as p_{rs}^{ul} increases, EE increases which is the same phenomenon with the case of SE. However, as Λ increases, increasing p_{rs}^{ul} helps little in improving EE, because the power supply drone consumes a lot of power.

Fig. 10 shows EE (bps/W) versus uplink RS power, p_{rs}^{ul}, when MF precoding is applied. In this case, reducing p_{rs}^{ul} is helpful to improve EE. Increasing p_{rs}^{ul} helps little in improving EE for the case of MF precoding because of the IUI limited situation.

Remark 6: With MF precoding, reducing uplink RS power in a certain level is always helpful to improve EE regardless of the number of required drones, Λ.

Remark 7: With ZF precoding, there is a downlink TX power that can optimize EE. On the other hand, with MF precoding, reducing TX power can give high benefit to increase EE due to IUI reduction.

Downlink TX power control is a very effective scheme to improve EE, because downlink TX power takes a large portion of power consumption in whole system. Fig. 11 presents SE (bps/Hz) versus downlink TX power, p_{tx}^{dl}, when ZF and MF precodings are applied in Case V and VI. It is obvious that increasing p_{tx}^{dl} increases SE, but the improvement for the case of MF precoding is not so dominant due to the IUI. However, this is not true for the case of EE. Fig. 12 shows EE (bps/W) versus downlink TX power, p_{tx}^{dl}, when ZF and MF precodings are applied in Cases V and VI. If we observe Case VI, with ZF precoding, as p_{tx}^{dl} increases, EE increases up to a certain point, then decreases. In the case of MF precoding, increasing p_{tx}^{dl} does little to help improve EE but reducing p_{tx}^{dl} is quite beneficial as we can see from Fig. 13. With ZF precoding, Case V-(a) shows 36.79% EE improvement (1.06 $\rightarrow$ 1.45 (Mbps/W)), Case V-(b) shows 43.06% EE improvement (0.72 $\rightarrow$ 1.03 (Mbps/W)), while Case VI shows 25.91% EE improvement (1.93 $\rightarrow$ 2.43 (Mbps/W)) by comparing the maximum EE with the minimum EE. With MF precoding, Case V-(a) shows 11.86% EE improvement (0.59 $\rightarrow$ 0.66 (Mbps/W)), Case V-(b) shows 7.14% EE improvement (0.42 $\rightarrow$ 0.45 (Mbps/W)), while Case VI shows 37.39% EE improvement (1.15 $\rightarrow$ 1.58 (Mbps/W)) by comparing the maximum EE with the minimum EE.

We summarize the observations of each case as follows:

- High clipping ratio reduces SE, and it causes EE loss.
- MF precoding is more robust than ZF precoding to clipping noise. There is a threshold clipping ratio, and ZF precoding has higher threshold than MF precoding.
- ICAF technique gives better performance gain when uplink RS power is small and MF precoding is used.
- With ZF precoding, increasing uplink RS power is beneficial to EE improvement for powered IoT devices. With

TABLE 4. EE gain of each case.

	Case I	Case II	Case III	Case IV	Case V-(a)	Case V-(b)	Case VI
ZF	6.25%	20.47%	51.43%	31.72%	36.79%	43.06%	25.91%
MF	25.47%	25.83%	3.45%	93.33%	11.86%	7.14%	37.39%

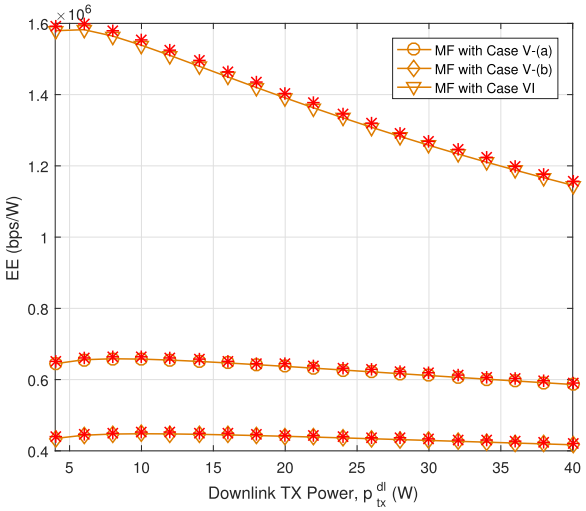

FIGURE 13. EE (bps/W) versus downlink TX power, p_{tx}^{dl}, when MF precoding is applied in Case V and VI, $M = 400$, $K = 40$.

MF precoding, controlling uplink RS power helps little to EE improvement for powered IoT devices.

- Reducing uplink RS power can be helpful for battery-limited IoT devices regardless of ZF and MF precoding.
- With ZF precoding, when the number of required drones, Λ is small, increasing uplink RS power improves EE.
- With MF precoding, reducing uplink RS power to a certain level is always helpful to improve EE regardless of the number of required drones, Λ.
- With ZF precoding, there is a downlink TX power that can optimize EE.

The EE gain of each case is summarized in Table 4. In general, MF precoding shows better EE gain than ZF precoding when having high clipping distortion and/or low TX power. As we witnessed, the derived closed-form approximations of SE and EE are well-matched with the simulation results, and they can be used for various analysis of the SE and EE for massive MIMO-OFDM based IoT networks. The EE gains we showed in various scenarios can be helpful to get some operational ideas of high EE massive MIMO-OFDM based IoT networks.

VI. CONCLUSION

In this paper, we investigated the EE gain of massive MIMO-OFDM in battery-limited IoT networks. There are many parameters that can be adjusted to increase the EE of massive MIMO based IoT networks. We derived the closed-form approximations of SE and EE to provide the performance gains of various scenarios. The scenarios include the cases of applying clipping PAPR reduction that causes clipping distortion noise, applying uplink RS power control that causes channel estimation error, applying downlink power control that causes SE loss, and the utilization of a power supply drone to extend the battery time of distributed IoT devices. We showed that the derived closed-form approximations of SE and EE are well-matched with the simulation results, and thus the closed-form approximations can be used as useful tools to design high EE massive MIMO-OFDM based battery limited IoT networks.

REFERENCES

[1] B. M. Lee and H. Yang, "Massive MIMO for industrial Internet of Things in cyber-physical systems," *IEEE Trans. Ind. Informat.*, vol. 14, no. 6, pp. 2641–2652, Jun. 2018.
[2] B. M. Lee, "Calibration for channel reciprocity in industrial massive MIMO antenna systems," *IEEE Trans. Ind. Informat.*, vol. 14, no. 1, pp. 221–230, Jan. 2018.
[3] B. M. Lee, "Energy efficient selected mapping schemes based on antenna grouping for industrial massive MIMO-OFDM antenna systems," *IEEE Trans. Ind. Informat.*, to be published, doi: 10.1109/TII.2018.2803118.
[4] T. L. Marzetta, "Noncooperative cellular wireless with unlimited numbers of base station antennas," *IEEE Trans. Wireless Commun.*, vol. 9, no. 11, pp. 3590–3600, Nov. 2010.
[5] E. Björnson, E. G. Larsson, and T. L. Marzetta, "Massive MIMO: Ten myths and one critical question," *IEEE Commun. Mag.*, vol. 54, no. 2, pp. 114–123, Feb. 2016.
[6] T. L. Marzetta, "Massive MIMO: An introduction," *Bell Labs Tech. J.*, vol. 20, pp. 11–22, Mar. 2015.
[7] L. Lu, G. Y. Li, A. L. Swindlehurst, A. Ashikhmin, and R. Zhang, "An overview of massive MIMO: Benefits and challenges," *IEEE J. Sel. Topics Signal Process.*, vol. 8, no. 5, pp. 742–758, Oct. 2014.
[8] F. Rusek *et al.*, "Scaling up MIMO: Opportunities and challenges with very large arrays," *IEEE Signal Process. Mag.*, vol. 30, no. 1, pp. 40–60, Jan. 2013.
[9] B. M. Lee, "Simplified antenna group determination of RS overhead reduced massive MIMO for wireless sensor networks," *Sensors*, vol. 18, no. 1, p. 84, Jan. 2018.
[10] B. M. Lee and Y. Kim, "Interference-aware PAPR reduction scheme to increase the energy efficiency of large-scale MIMO-OFDM systems," *Energies*, vol. 10, no. 8, p. 1184, Aug. 2017.
[11] T. Jiang and Y. Wu, "An overview: Peak-to-average power ratio reduction techniques for OFDM signals," *IEEE Trans. Broadcast.*, vol. 54, no. 2, pp. 257–268, Jun. 2008.
[12] X. Lu, P. Wang, D. Niyato, D. I. Kim, and Z. Han, "Wireless networks with RF energy harvesting: A contemporary survey," *IEEE Commun. Surveys Tuts.*, vol. 17, no. 2, pp. 757–789, 2nd Quart., 2015.
[13] E. Eraslan and B. Daneshrad, "Low-complexity link adaptation for energy efficiency maximization in MIMO-OFDM systems," *IEEE Trans. Wireless Commun.*, vol. 16, no. 8, pp. 5102–5114, Aug. 2017.
[14] B. M. Lee, Y. S. Rim, and W. Noh, "A combination of selected mapping and clipping to increase energy efficiency of OFDM systems," *PLoS ONE*, vol. 12, no. 10, p. e0185965, Oct. 2017.
[15] B. M. Lee, "Energy efficiency gain of cellular base stations with large-scale antenna systems for green information and communication technology," *Sustainability*, vol. 9, no. 7, p. 1123, Jul. 2017.
[16] B. M. Lee and Y. Kim, "Design of an energy efficient future base station with large-scale antenna system," *Energies*, vol. 9, no. 12, p. 1083, Dec. 2016.

[17] J. Xu and L. Qiu, "Energy efficiency optimization for MIMO broadcast channels," *IEEE Trans. Wireless Commun.*, vol. 12, no. 2, pp. 690–701, Feb. 2013.
[18] E. Björnson, J. Hoydis, M. Kountouris, and M. Debbah, "Massive MIMO systems with non-ideal hardware: Energy efficiency, estimation, and capacity limits," *IEEE Trans. Inf. Theory*, vol. 60, no. 11, pp. 7112–7139, Nov. 2014.
[19] M. Zorzi, A. Gluhak, S. Lange, and A. Bassi, "From today's Intranet of Things to a future Internet of Things: A wireless- and mobility-related view," *IEEE Wireless Commun.*, vol. 17, no. 6, pp. 44–51, Dec. 2010.
[20] J. Duan, D. Gao, D. Yang, C. H. Foh, and H.-H. Chen, "An energy-aware trust derivation scheme with game theoretic approach in wireless sensor networks for IoT applications," *IEEE Internet Things J.*, vol. 1, no. 1, pp. 58–69, Feb. 2014.
[21] P. Kamalinejad, C. Mahapatra, Z. Sheng, S. Mirabbasi, V. C. M. Leung, and Y. L. Guan, "Wireless energy harvesting for the Internet of Things," *IEEE Commun. Mag.*, vol. 53, no. 6, pp. 102–108, Jun. 2015.
[22] J. Xu and R. Zhang, "A general design framework for MIMO wireless energy transfer with limited feedback," *IEEE Trans. Signal Process.*, vol. 64, no. 10, pp. 2475–2488, May 2016.
[23] Y. Zeng and R. Zhang, "Energy-efficient UAV communication with trajectory optimization," *IEEE Trans. Wireless Commun.*, vol. 16, no. 6, pp. 3747–3760, Jun. 2017.
[24] L. Da Xu, W. He, and S. Li, "Internet of Things in industries: A survey," *IEEE Trans. Ind. Informat.*, vol. 10, no. 4, pp. 2233–2243, Nov. 2014.
[25] W. Wolf, "Cyber-physical systems," *Computer*, vol. 42, no. 3, pp. 88–89, 2009.
[26] E. A. Lee, "Cyber physical systems: Design challenges," in *Proc. 11th IEEE Int. Symp. Object Oriented Real-Time Distrib. Comput. (ISORC)*, May 2008, pp. 363–369.
[27] R. R. Rajkumar, I. Lee, L. Sha, and J. Stankovic, "Cyber-physical systems: The next computing revolution," in *Proc. 47th Design Autom. Conf. (DAC)*, Jun. 2010, pp. 731–736.
[28] T. L. Marzetta, E. G. Larsson, H. Yang, and H. Q. Ngo, *Fundamentals of Massive MIMO*. London, U.K.: Cambridge Univ. Press, 2016.
[29] R. O'Neill and L. B. Lopes, "Envelope variations and spectral splatter in clipped multicarrier signals," in *Proc. IEEE Int. Symp. Pers., Indoor Mobile Radio Commun. (PIMRC)*, Toronto, ON, Canada, vol. 1, Sep. 1995, pp. 71–75.
[30] B. M. Lee and R. J. P. de Figueiredo, "Adaptive predistorters for linearization of high-power amplifiers in OFDM wireless communications," *Circuits, Syst. Signal Process.*, vol. 25, no. 1, pp. 59–80, Feb. 2006.
[31] J. Armstrong, "Peak-to-average power reduction for OFDM by repeated clipping and frequency domain filtering," *Electron. Lett.*, vol. 38, no. 5, pp. 246–247, Feb. 2002.
[32] J. J. Bussgang, "Cross correlation functions of amplitude distorted Gaussian signals," Res. Lab. Electron., Tech. Rep. 216, Mar. 1952, pp. 1–14.
[33] H. Ochiai and H. Imai, "Performance of the deliberate clipping with adaptive symbol selection for strictly band-limited OFDM systems," *IEEE J. Sel. Areas Commun.*, vol. 18, no. 11, pp. 2270–2277, Nov. 2000.
[34] H. Ochiai and H. Imai, "Performance analysis of deliberately clipped OFDM signals," *IEEE Trans. Commun.*, vol. 50, no. 1, pp. 89–101, Jan. 2002.
[35] B. M. Lee and Y. Kim, "An adaptive clipping and filtering technique for PAPR reduction of OFDM signals," *Circuits Syst. Signal Process.*, vol. 32, no. 3, pp. 1335–1349, Jun. 2013.
[36] S. C. Cripps, *RF Power Amplifiers for Wireless Communications*, 2nd ed. Norwood, MA, USA: Artech House, 2006.
[37] S. L. Miller and R. J. O'Dea, "Peak power and bandwidth efficient linear modulation," *IEEE Trans. Commun.*, vol. 46, no. 12, pp. 1639–1648, Dec. 1998.
[38] H. Yang and T. L. Marzetta, "Performance of conjugate and zero-forcing beamforming in large-scale antenna systems," *IEEE J. Sel. Areas Commun.*, vol. 31, no. 2, pp. 172–179, Feb. 2013.
[39] H. Yang and T. L. Marzetta, "Total energy efficiency of cellular large scale antenna system multiple access mobile networks," in *Proc. IEEE Online Conf. Green Commun. (GreenCom)*, Piscataway, NJ, USA, Oct. 2013, pp. 27–32.
[40] H. Yang and T. Marzetta, "Energy efficient design of massive MIMO: How many antennas?" in *Proc. IEEE 81st Veh. Technol. Conf.*, Glasgow, U.K., May 2015, pp. 1–5.
[41] E. Dahlman, S. Parkvall, and J. Skold, *4G: LTE/LTE-Advanced for Mobile Broadband*. New York, NY, USA: Academic, 2011.
[42] S. Ahmadi, *LTE—Advanced: A Practical Systems Approach to Understanding 3GPP LTE Releases 10 and 11 Radio Access Technologies*, 1st ed. Cambridge, MA, USA: Academic, 2013.
[43] S. Sesia, I. Toufik, and M. Baker, *LTE—The UMTS Long Term Evolution: From Theory to Practice*, 2nd ed. Hoboken, NJ, USA: Wiley, 2011.
[44] S. Wagner, R. Couillet, M. Debbah, and D. T. M. Slock, "Large system analysis of linear precoding in correlated MISO broadcast channels under limited feedback," *IEEE Trans. Inf. Theory*, vol. 58, no. 7, pp. 4509–4537, Jul. 2012.
[45] "Radio frequency (RF) requirements for LTE pico node B," ETSI, Sophia Antipolis, France, Tech. Rep. 136.931, 2012.

BYUNG MOO LEE (M'05) received the Ph.D. degree in electrical and computer engineering from the University of California, Irvine, CA, USA, in 2006. He had 10 years of industrial experience including research positions with the Samsung Electronics Seoul R&D Center, Samsung Advanced Institute of Technology, and Korea Telecom R&D Center. He is currently an Assistant Professor with the School of Intelligent Mechatronics Engineering, Sejong University, Seoul, South Korea. He participated in IEEE 802.16/11, Wi-Fi Alliance, and 3GPP LTE standardizations, and also participated in Mobile VCE and Green Touch Research Consortiums, where he made numerous contributions and filed a number of related patents. His research interests are in the areas of wireless communications, signal processing, and machine learning applications.

Dr. Lee served as the Vice Chairman for the Wi-Fi Alliance Display MTG from 2015 to 2016.